Raman spectroscopic and magnetic properties of Europium doped nickel oxide nanoparticles prepared by microwave-assisted hydrothermal method

Wilfrid Prellier, Ranjith Kumar P, Neena Prasad, Fabien Veillon

Version of Record: https://www.sciencedirect.com/science/article/pii/S0925838820340032
Manuscript_7a75c5ff0a3d1ae0f8ef33169a0c0ec0

Raman spectroscopic and magnetic properties of Europium doped Nickel oxide nanoparticles prepared by microwave-assisted hydrothermal method

Ranjith Kumar P [a], Neena Prasad [b], Fabien Veillon [c], Wilfrid Prellier [c, #]

[a] *Materials Research Centre, Indian Institute of Science, Bangalore 560 012, India*

[b] *Nanophotonics Laboratory, Department of Physics, National Institute of Technology, Tiruchirappalli, 620 015 India*

[c] *Laboratoire CRISMAT, CNRS UMR 6508, ENSICAEN, Normandie Université, 6 Bd Maréchal Juin, F-14050 Caen Cedex 4, France*

[#] Corresponding author: e-mail addresses: wilfrid.prellier@ensicaen.fr (Wilfrid Prellier)

Abstract

Pure and 5 mol% Eu doped nickel oxide (NiO) nanoparticles were synthesized by microwave-assisted hydrothermal method. X-ray diffraction and Rietveld refinement analysis confirmed the phase and purity of prepared nanoparticles. Scanning electron microscopy analysis revealed that the undoped nanoparticles are porous flake-like structures while the doped samples were aggregated. X-ray photoelectron spectroscopy analysis disclosed that Eu doping increases hole concentration, Ni^{2+} vacancies, and defective oxygen concentration in the nanoparticles. The magnetic analysis shows the presence of weak ferromagnetism in lower fields of the undoped nanoparticles. On doping with Eu, the ferromagnetic behavior increases due to increased oxygen defects and uncompensated surface spins. Raman spectroscopy investigation shows the absence of 2M vibrational mode and reduced antiferromagnetic coupling in the prepared samples. It also substantiated the presence of defects in the prepared samples. Eu doping produced local vibrations that overlap with SO mode of NiO and shifting of 1M band due to its higher mass. Eu dopant can modify the magnetic property of NiO nanoparticles that can be used in spintronic applications.

Key words: Nickel oxide, Europium, defects, ferromagnetism, Raman spectroscopy.

1. Introduction

Nanoparticles are extensively studied since they exhibit highly attractive and unusual properties, due to the more significant surface electrons and surface and interface effects than the bulk materials [1]. Nickel oxide (NiO) is an extensively studied magnetic material since it manifests room temperature antiferromagnetic behaviour with high Neel temperature (T_N = 523 K) in bulk form. But, when the particle size is reduced to the nanoscale regime, NiO shows unique and exciting properties like high charge mobility, high sensing, good photocatalytic activity, etc. [2-5]. The remarkable change in properties is due to the quantum size effect, surface effect, shape, and volume effects [6, 7]. When doped with other metals, like Mn, Fe, Cu, Ce, etc., NiO nanoparticles show drastic changes in the magnetic and optical properties [8-11]. Also, the synthesis route can cause considerable changes in the electronic structure of NiO nanoparticles [12, 13]. Hence, NiO nanoparticles of various size, shape, and different dopants have been synthesized by different methods, and its potential application in numerous fields have been studied [8, 14-18]. Since the rare earth elements possess partially filled 4f orbitals, these elements can be utilized as dopants to modulate NiO nanoparticles [19-23]. The structural, magnetic, optical, and dielectric behaviour of rare earth (Y, Pr, Sm, Gd, and Er) doped NiO nanoparticles were extensively studied by Al Boukhari et al. [11, 21-24]. Their investigation shows that rare earth doping increases the bandgap, dielectric constant, electrical conductivities, and magnetization in NiO nanoparticles. However, the effect of such dopants on the vibrational properties of the NiO nanoparticles was not reported. Naseem Siddique et al. have synthesized Ce^{3+} doped NiO nanoparticles by sol-gel method and explored the optical and magnetic properties [25]. They have reported that Ce^{3+} doping produces defects that shift and broaden the 1LO and 2LO vibration modes and suppresses the 2M magnon mode. Chauhan et al. have investigated the effect of Nd^{3+} dopant

on the optical properties of NiO nanoparticles prepared by the sol-gel method and reported the possible application for optical glucose sensors [20].

In all the reports mentioned above, weak ferromagnetism has been observed in the NiO nanoparticles when doped with rare earth elements. The origin of such weak ferromagnetism has been attributed to the presence of Ni vacancy, and photoluminescence results substantiated it. Among the rare earth metals, Europium (Eu) is known to be the most reactive one. It can exist as Eu^{3+} or Eu^{2+} in compounds. Eu^{2+} is formed in reduced conditions, and Eu^{3+} is known to exist as a more stable state in most compounds [26]. Goumri-Said et al. have investigated, theoretically and experimentally, the effect of Eu doping on the optical properties and crystal structure of NiO thin films [27]. It was found that the incorporation of Eu produced changes in the polarization of NiO, which affects the magnetic moment.

Microwave-assisted hydrothermal method is known for the rapid synthesis rate, increased chemical kinetics, higher yield, etc. [16, 28]. We have successfully synthesized pure and 5 mol% Eu-doped NiO nanoparticles by microwave assisted hydrothermal method in the present work. We have concentrated on investigating the effect of Eu doping on the vibrational and magnetic properties of NiO nanoparticles. The crystal structure, chemical state of the constituent elements, and morphology of the prepared nanoparticles were also examined.

2. Experimental details

2.1 Synthesis of the nanoparticles

Commercially available nickel acetate tetrahydrate ($Ni(CH_3COO)_2.4H_2O$) (Alfa Aesar, 98%), Sodium hydroxide (NaOH) (Alfa Aesar, 98%), and Europium acetate ($Eu(CH_3COO)_3$) (Sigma Aldrich, 99.9%) were used without further purification as precursors for the synthesis of the nanoparticles. Distilled water prepared in the laboratory was used throughout the

experiment. For the synthesis of nickel oxide (NiO) nanoparticles, $Ni(CH_3COO)_2.4H_2O$ and NaOH, in 1:2 molar ratio, were dissolved in 35 ml and 30 ml of distilled water, respectively. Then, the NaOH solution was added dropwise to $Ni(CH_3COO)_2$ solution under constant stirring. The obtained suspension was transferred to a 90 ml microwave reactor vessel and then placed on the turntable inside the microwave digestive system (CEM MARS 6) for uniform heating. At a heating rate of 5 °/min, the suspension was heated to 180 °C for 30 min and then allowed to cool naturally. The obtained product was washed with distilled water and ethanol several times by centrifugation to remove all unreacted ions from the products and dried in air at 180 °C for 3 hrs. It was then manually ground into a fine powder using agate mortar, secured using platinum crucible, and annealed in a muffle furnace at 400 °C for 3 hrs. The heating rate was kept constant at 5 °/min, and cooling was done naturally.

For the synthesis of Eu doped NiO nanoparticles, 5 mol% of $Eu(CH_3COO)_3$ was used as Eu source, and a similar procedure was adopted. The obtained final products were NiO and $Ni_{0.95}E_{0.5}O$, respectively, and used for further characterizations.

2.2 Characterization

The phase and crystallinity of the synthesized nanoparticles were analyzed by the X-ray diffraction (XRD) technique using the PanAlytical X'pert Pro X-ray diffractometer having Cu K_α (λ = 1.5418 Å) source. The XRD patterns in the 2θ range of 20 - 90° were obtained at a step size of 0.025°/sec. Chemical oxidation states of the nanoparticles were investigated by X-ray photoelectron spectroscopy (XPS) (Kratos Axis Ultra DLD) with monochromatic Al Kα radiation (1486.8 eV). Before recording the spectra, the binding energies were calibrated with reference to adventitious carbon 1s peak at 284.6 $\pm$ 0.1 eV. The morphology and composition of the nanoparticles were examined by high-resolution field emission scanning electron microscopy (FE-SEM, Carl ZEISS-Ultra55) equipped with energy-dispersive X-ray

spectroscopy (EDS). Magnetization measurements were conducted using a superconducting quantum interference device (SQUID, Quantum design) magnetometer between a magnetic field of -60 to +60 kOe. Micro Raman spectra were obtained using LabRAM HR800 Raman spectrometer equipped with diode-pumped solid-state laser (Quantum MPC 6000) working at 532 nm wavelength. The laser was operated at a power of 50 mW, and the spectra were obtained in the wavenumber range of 250 - 1600 cm^{-1}. The instrument was calibrated concerning Si-Si vibration mode at 520 $\pm$ 0.25 cm^{-1}. All measurements were performed at room temperature.

3. Results and discussion

3.1 Structure and morphological analysis

Figure 1 shows the refined XRD patterns of the synthesized nanoparticles. The diffraction pattern of the undoped (NiO) and doped ($Ni_{0.95}E_{0.5}O$) samples show five distinct peaks. These peaks correspond to (111), (200), (220), (311), and (222) orientations of the FCC crystal structure that belongs to the Fm-3m space group [21, 25, 29]. The crystallinity and purity of the NiO nanoparticles can be confirmed from the high-intensity narrow peaks and the absence of impurity peaks. In the case of $Ni_{0.95}E_{0.5}O$ nanoparticles, no characteristic peaks of Europium compounds can be found, suggesting that the Eu ions are successfully integrated into NiO lattice [21-23]. Rietveld analysis, done using the MAUD program [30], corroborates these observations. From the diffraction patterns, we can perceive that the $Ni_{0.95}E_{0.5}O$ nanoparticles have broader peaks and relatively lower intensity than the pure NiO nanoparticle. This variation in intensity and peak width indicates that the crystallinity of the $Ni_{0.95}E_{0.5}O$ nanoparticles has decreased compared to the undoped samples, which complies with the results reported in the literature [21-24].

Likewise, it can be noticed that the relative intensity of the peaks corresponding to (311) and (222) orientations have decreased, which signifies that doping with Eu atoms disrupts the growth of NiO crystals along with those directions. While examining the peak positions, it was observed that the peaks corresponding to (111) and (200) orientations of the $Ni_{0.95}E_{0.5}O$ nanoparticles have been shifted by 0.06° and 0.03°, respectively, towards the lower angle, compared to the pure NiO nanoparticles. Since the atomic radius of Eu^{3+} (0.0947 nm) is more significant than Ni^{2+} (0.069 nm), the lattice will undergo distortion on Eu substitution. The distortion in the lattice will cause tensile stress in the crystals, which causes the peak to shift towards the lower angle. Also, the peak shift towards the lower angle indicates that the lattice parameter has increased [25]. A standard LaB_6 sample was used to determine the instrumental line broadening of each peak. The average crystallite size (*D*) of both the samples was calculated from the three high-intensity peaks, i.e., (111), (200), and (220), using the Scherrer equation given by [31],

$$D = \frac{K\lambda}{\beta cos\theta} \tag{1}$$

where, the shape factor K = 0.9, λ is the wavelength of the X-ray, β is the full width half maximum (FWHM) at the Bragg angle θ. The lattice parameter (*a*) was estimated using the expression 2 [27] for the cubic crystal system,

$$\frac{1}{d_{hkl}^2} = \frac{h^2 + k^2 + l^2}{a^2} \tag{2}$$

where, d is the interplanar spacing, and h k l are the Miller indices. The lattice strain (*ε*) was estimated using equation 3 [31],

$$\varepsilon = \frac{\beta}{4\ tan\theta} \tag{3}$$

The estimated average crystallite size for the NiO and $Ni_{0.95}E_{0.5}O$ samples were 13.45 and 6.51 nm, respectively. The lattice strain was found to be 0.0066 and 0.0138 for the NiO and $Ni_{0.95}E_{0.5}O$ nanoparticles, respectively. The calculated lattice parameter was 4.179 Å and 4.184 Å, for the NiO and $Ni_{0.95}E_{0.5}O$ nanoparticles. With the uncertainty of $\pm$0.004 Å, the obtained values are in good agreement with reported literature [21-24]. It can be observed that Eu doping has decreased the lattice parameter value and reduced the crystallite size by 50% as compared to the pure NiO nanoparticles. Similar results were reported when NiO nanoparticles were doped with other rare earth elements [21-25]. The decrease in size increases the surface area to volume ratio, which causes remarkable changes in the properties of the material [6, 7, 29, 32]. Rinaldi-Montes et al. have investigated the effect of NiO nanoparticles size on the T_N by neutron diffraction experiment [33]. Their analysis shows that the T_N of NiO nanoparticles decreases when the size is reduced. Popkov et al. reported that the decrease in the size of the NiO nanoparticles increases the ferromagnetic contribution. When the size of the nanoparticle is reduced, the fraction of surface atoms increases, which in turn increases the uncompensated surface spins [34].

Figure 2 shows the high magnification FE-SEM micrographs and the corresponding EDS spectra of the pure NiO and $Ni_{0.95}E_{0.5}O$ nanostructures. The NiO nanoparticles (Figure 2(a)) were found to be perforated flakes of different shapes and various sizes with an average thickness of about 15 nm. Since the particles can be distinguished individually with clearly visible boundaries, their sizes can be determined from image analysis [35]. The size of the flakes varies from 30 to 230 nm, with the more significant number of particles being in the 90 – 150 nm range. The average size of the particle was found to be 120 nm (Figure 2(e)). The size of the pores varies from 3 to 12 nm based on the size of the flakes. The larger size can be due to the aggregation of the crystallites during synthesis. This flake-like morphology observed in NiO nanoparticles synthesized by microwave-assisted route is due to oriented

attachment [17, 36]. Similar flake-like mesoporous NiO nanoparticles were prepared by Zhang et al. by hydrothermal method using nickel chloride as a precursor, and its potential application as NO_2 gas sensor has been explored [18]. The relatively bigger size and porous structure compared to those reported in the literature can be attributed to longer synthesis time. The nucleation rate and growth of the NiO nanoflakes are augmented by microwaves during the synthesis. When exposed to microwave for a longer duration, the neighbouring nanoparticles aggregate and grow along a specific direction and form nanoflakes [17]. Thus, the porous structures might be due to the incomplete aggregation of the nanoparticles and perhaps the evaporation of water molecules during annealing in air. When doped with Eu, we can observe considerable changes in the morphology of the nanoparticles. The flake size appears to be reduced, and the particles are agglomerated, as seen in Figure 2(c). This non-uniform shape and highly agglomerated morphology changes from almost uniform, and less agglomerated particles might minimise the surface energy [36]. Such accumulation of nanoparticles was also observed when NiO nanoparticles were doped with rare earth elements like Pr, Sm, Gd, Er, etc. [21-24]. These observations indicate that doping causes aggregation of the nanoparticles and increases the interaction between them. This accumulation might be prevented by using appropriate surfactants. Synthesis of NiO nanoparticles by wet chemical routes is characterised by a large number of Ni^{2+} vacancies and a higher surface to volume ratio [37]. The presence of defects greatly affects the electrical, magnetic, and properties of the oxide nanostructures [21-25].

3.2 Compositional analysis

EDS was performed over 30 μm × 30 μm to estimate the atomic percentage of constituent elements present in the samples. The EDS spectra (Figure 2(b) and (d)) confirms the presence of Ni and O elements in the prepared samples and the existence of the Eu element along with Ni and O in the doped sample. The atomic % of constituent elements present in the samples

are shown in the table given in the inset of each EDS spectra. The atomic percentage ratio of [Eu] to [Ni] was estimated to be 4.56 in the $Ni_{0.95}E_{0.5}O$ sample, which is very close to the amount of dopant concentration (5 mol%) used during synthesis. Also, the absence of other elements confirms the phase purity of the prepared samples.

The prepared nanoparticles were characterised by XPS, which gives the elemental composition and their oxidation states at a depth of a few atomic layers' thicknesses from the surface. Figures 3 and 4 show the obtained core level XPS spectra of constituent elements present in the pure NiO and $Ni_{0.95}E_{0.5}O$ samples. Peak fittings were carried out using CasaXPS software with Shirley's background. The peaks were deconvoluted using the Gaussian-Lorentzian function. The details of the position, FWHM, and area of the peaks are summarised in Table 2.

Due to the complexity of the 2p spectrum, it is challenging to analyse the chemical state of nickel oxide and nickel hydroxide [38]. In the present work, the oxidation states have been assigned from the binding energies of Ni $2p_{3/2}$ spectra, which is generally used as the fingerprint of NiO [39]. On deconvolution, the acquired core level spectra of Ni $2p_{3/2}$ yields four peaks, characteristic central peak with a shoulder at ~ 1.5 eV and two satellite peaks at a higher binding energy level [38, 39]. These peaks that are intrinsic for nickel oxide can be observed in both NiO and $Ni_{0.95}E_{0.5}O$ samples (Figures 3(a) and 4(a)). The central peak at 853.8 eV is due to the local screening effect, which gives rise to $3d^9$ ligand band hole at the core level site induced by the X-ray photons. The shoulder peak at 855.5 eV is due to the surface and non-local screening effects [38, 39]. The 2p core hole formation and the corresponding charge transfer process that causes screening of the core hole is accompanied by d-d transitions, which produces the shake-up peaks at 860.8 and 864.1 eV [40]. The deconvolution of the spectrum of $Ni_{0.95}E_{0.5}O$ sample yields peaks located at 854.0, 855.7, 861.1, and 865.1 eV. Thus, when doped with Eu, these peaks are shifted to a higher binding

energy side. Since the doping of Eu atoms distorts the lattice, it creates an asymmetry in the electron cloud over the neighbouring atoms. This changes the bond length and hence increases the binding energy [41]. We can also observe that the area of all the peaks has decreased by almost half after doping. The ratio of the area of the shoulder peak with respect to the main peak has decreased when doped with Eu atoms. This decrease might be due to the decrease in the Ni 3d – O 2p hybridization in the nanoparticles, which in turn decreases the covalency and electron-phonon coupling [12]. The FWHM of the shake-up peaks has increased when doped with Eu, indicating that the concentration of the holes has increased. The number of surface atoms and the Ni^{2+} vacancies in the $Ni_{0.95}E_{0.5}O$ nanoparticles increases due to particle size reduction. Since each Ni^{2+} vacancy gives rise to two holes, the concentration of holes increases when doped with Eu atoms.

Deconvolution of O 1s spectrum yields three peaks located at 528.7, 530.4, and 531.7 eV for the pure NiO sample (Figure 3(b)). These peaks correspond to the lattice oxide, defective oxygen, and adsorbed water, respectively [39, 42]. Whereas, in the case of $Ni_{0.95}E_{0.5}O$ sample, the deconvoluted O 1s spectrum yields two peaks located at 528.8 and 530.6 eV (Figure 4(b)). The shift towards higher binding energy might be due to the higher electronegativity of Ni, which increases the Eu-O bond ionicity [43]. It can be observed that doping causes broadening and an increase in the intensity of the defective oxygen peak. Also, the peak area of the defective oxygen has doubled after doping. Thus, when doped with Eu, the defective oxygen (the neighbouring oxygen atoms of Ni vacancy) concentration increases. Hence, we can deduce that the number of Ni vacancies has increased in $Ni_{0.95}E_{0.5}O$ nanoparticles. The acquired core level 3d spectrum of Eu yields two characteristic peaks that arise due to sizeable spin-orbit coupling (Figure 4(c)). The two peaks located at 1133.8 and 1163.8 eV, which correspond to Eu $3d_{5/2}$ and Eu $3d_{3/2}$, respectively, are due to the trivalent $4f^6$ configuration [43, 44]. Zhang et al. have reported oxygen vacancies in Eu_2O_3 microwires

that give rise to unusual magnetic properties [45]. Thus, we can presume that the enhancement in oxygen vacancy concentration in the $Ni_{0.95}E_{0.5}O$ nanoparticles might be from the contribution of Eu atoms present in the nanoparticles.

3.3 Magnetic analysis

Defective structures, doping, and finite-size effects cause the magnetic moment in most of the antiferromagnetic nanoparticles. NiO nanoparticles exhibit anomalous magnetic properties due to their finite size effect, where the uncompensated surface spins cause changes in the magnetic order [6, 7, 46]. Figure 5 shows the hysteresis loop of the synthesized pure NiO and $Ni_{0.95}E_{0.5}O$ nanoparticles. The M - H curve of pure NiO (figure 5a) shows an almost linear response with a low degree of magnetisation and low hysteresis loss, which is the typical behaviour of NiO nanoparticles when the size is reduced. Since no impurities were observed form XRD and EDS analysis, the presence of weak ferromagnetism in the pure NiO nanoparticles at the low field region can be attributed to vacancies in the prepared nanoparticles [21]. The remnant magnetization (M_r) and coercivity (H_c) were 113.5×10^{-5} emu/g and 0.195 kOe, respectively. The relatively higher coercivity is due to exchange coupling between uncompensated surface spins and antiferromagnetic core [7].

On doping with Eu, the hysteresis response of the sample shows drastic changes (figure 5b). The linearity has impaired, and an increase in M_r (113.1×10^{-3} emu/g) by two orders of magnitude and H_c (0.198 kOe) by a small value can be observed. Likewise, the hysteresis loss is high as compared to the undoped NiO nanoparticles. When the nanoparticles are in close contact, the exchange interaction is increased. As observed from FE-SEM micrographs, the particles are agglomerated when doped with Eu. Thus, when doped with Eu atoms, linear behaviour is impaired, and the rate of magnetization has increased significantly. Similar

results were obtained by Al Boukhari et al. when NiO nanoparticles were doped with rare earth elements like Y, Pr, Sm, Gd, and Er [21]. Their analysis shows that the ferromagnetic behaviour of the rare earth doped NiO nanoparticles depends on the type of dopant used. Depending on the dopant element, the vacancies in the NiO nanoparticles varies. Also, the reduction in the size of the particles that result in a higher number of exchange bonds being broken on the particle surface can affect the magnetization [47]. Such broken exchange bonds give rise to many uncompensated spins and hence increases the exchange coupling. Similar results were obtained by Ponnusamy et al. and Moura, K. O., et al. when Fe-doped NiO nanoparticle was synthesized by the wet-chemical route [10]. Their results suggest that the linear behaviour was due to the contribution of uncompensated surface spins to the magnetization. Also, the free electrons from the higher valent dopant can contribute to the exchange interactions. The change in magnetic properties might be due to Eu^{3+} bonding with O, which gives rise to a more significant number of oxygen vacancies [45]. As observed from XPS analysis, the oxygen vacancy concentration has increased when doped with Eu. The incorporation of Eu^{3+} ions in NiO induces ferromagnetism by polarizing the adjoining vacancy atoms [25]. Goumri-Said et al. have reported that when Eu is incorporated into the NiO matrix, it undergoes spin polarization, and hence the magnetization is increased. Because of the presence of the Eu impurity, the magnetic moment of the Ni atoms changes such that the Ni atoms closer to the Eu atom have higher magnetic moments, and this, in turn, induces magnetic moment in oxygen atom [27]. Thus, the magnetic property of the NiO nanoparticles can be altered not only by varying the size but also by doping with different rare earth elements.

3.3 Raman analysis

Raman spectroscopy is an effective non-destructive material characterization technique that commonly demonstrates the structural arrangements, crystallographic orientations, structural

defects, doping effects, lattice disorder, etc. [48-50]. Moreover, Raman spectroscopy can be successfully utilized to probe the doping effect and local vibrational modes, electro-phonon coupling, spin-phonon coupling, etc. [51-53]. Figure 6 shows the recorded room temperature Raman spectra of the prepared pure NiO and $Ni_{0.95}E_{0.5}O$ nanostructures within the range from 250 to 1300 cm^{-1}. The spectra are deconvoluted using multiple Lorentzian fits. The Raman band below 600 cm^{-1} is generally owing to first-order phonon scattering, and the peaks above 600 cm^{-1} are due to second-order scattering [14]. The deconvolution of the undoped NiO nanoparticles spectrum gives eight peaks (Figure 6a), which are the characteristic Raman mode vibration of face-centered cubic NiO nanostructures. In detail, the Raman bands observed at 368, 445, 537, 666, 827, 937, 1048, and 1140 cm^{-1} are corresponding to one phonon (1P) transverse optical (TO) modes, surface optical (SO) modes, 1P longitudinal optical (LO) mode, two-phonon (2P) TO (730), 2P LO+TO, 2P SO, the vibrational origin of 2LO and one-magnon (1M) bands respectively [9]. The obtained Raman active mode is in good accordance with the reported characteristic phonon mode of vibrations of intrinsic NiO nanostructures [32, 54, 55]. Hence, from the Raman spectral analysis, the phase purity of the prepared NiO nanoflakes can be confirmed.

The appearance of 1P SO mode suggests that the prepared nanoparticles are imperfect [32]. Moreover, the appearance of 1P LO and TO are usually originated from the parity breaking defects in NiO, which arises due to the nickel vacancy concentration [56]. The presence of defects and surface-induced disorder and the imperfectness of the prepared nanoflakes can also be the reason for the appearance of 1LO [9]. Oftentimes, NiO exhibits a 2M band that supports the existence of the antiferromagnetic state of pure NiO nanostructures at room temperature due to the dominant superexchange interaction mechanism between the next-nearest-neighbouring Ni ions through O in the Ni^{2+}-O^{2-}-Ni^{2+} linear atomic chain [54, 57]. Ulamne et al. reported the reduction of 2M mode and complete vanishing of 2M with a

decrease in particle size and for crystallite size below 100 nm, respectively [58, 59]. Finite-size effect, smaller crystallites, and disorder-induced defects can reduce spin correlation length that can be a reason for the reduction and vanishing of 2M modes in NiO nanostructures [32, 54, 59].

Moreover, two types of magnons associated with the spin up and spin down of two electrons can be observed in the case of bulk antiferromagnetic NiO [14]. 2M is significant to probe the magnetic domain structure since it is well separated from phonon contribution and the elastic scattering line [60]. The transition from antiferromagnetic to ferromagnetic nature NiO leads to the disappearance of 2M peaks since the magnon has a strong dependence on the magnetic nature of NiO [14]. Interestingly, in the present investigation, there was no sign of the appearance of the 2M band was observed in the Raman spectra of undoped NiO nanoparticles. The absence of the 2M band indicates the substantial antiferromagnetic coupling reduction with an average crystallite size of 13.45 nm and particle size ~120 nm [58]. Hence, we can conclude that the absence of magnon peak in the Eu-doped NiO nanoparticles might be due to the presence of uncompensated surface spins, smaller crystallite size, disorder-induced defects that result in the reduction of spin correlation between the next nearest neighbour Ni^{2+} ions in the crystal lattice and hence, the reduction in antiferromagnetic coupling strength [54, 59, 61, 62].

The deconvolution of $Ni_{0.95}E_{0.5}O$ spectrum gives seven distinct peaks around 361, 537, 678, 841, 946, 1040 and 1138 cm^{-1} (Figure 5(b)). From the peak positions, it can be observed that the 1P TO band is shifted from 368 to 361 cm^{-1} when doped with Eu. This slight shift can be associated with the vacancies and structural defects of the nanostructure [9, 63]. Since doping with Eu increases the number of oxygen vacancies as noticed from XRD and XPS analysis, this observation is in good accordance with the results. Also, we can observe a small shift in the 2LO mode when doped with Eu, which can be due to a reduction in crystallite size.

Furthermore, the 1P modes of the $Ni_{0.95}E_{0.5}O$ nanostructures were found to be broadened, and the Raman band from 820 to 1150 cm^{-1} found to have asymmetry in the lower wavenumber region as compared with the undoped NiO nanostructures. This change can be due to the reduction of phonon lifetime in the nanocrystalline regime [50]. Usually, a band centered around 450-550 cm^{-1} that were quite rarely perceived in the Raman spectrum for Eu-doping into metal oxides [64]. This band is generally attributed to local vibrational mode (LVM), which is purely a dopant induced vibrational mode. When Nickel or oxygen lattice sites are substituted with Eu-dopant, dopant related LVM might appear in the Raman spectra of the Eu doped NiO nanoflakes along with the characteristic modes of pure NiO [65]. According to the harmonic approximation, the frequency of LVM can be written as [61],

$$\frac{\omega_{NiO}}{\omega_{LVM}} = \left(\frac{\mu_{LVM}}{\mu_{NiO}}\right)^{1/2} \quad \text{..... (4)}$$

The above expression can write as in terms of wavenumber as,

$$\frac{\bar{\upsilon}_{NiO}}{\bar{\upsilon}_{LVM}} = \left(\frac{\mu_{LVM}}{\mu_{NiO}}\right)^{1/2} \quad \text{..... (5)}$$

The average effective mass model can be introduced,

$$\mu_{Eu-Ni\,(LVM)} = \frac{(\mu_{Eu-Ni}+\mu_{Eu-Eu})}{2} \text{ ..... (6)}$$

Or

$$\mu_{Eu-O(LVM)} = \frac{(\mu_{Eu-O}+\mu_{Eu-Eu})}{2} \text{ ..... (7)}$$

Both the Eu-Ni and Eu-O separately contribute to the effective mass; hence the Eu dopant can occupy either Ni or O sites and produce two different LVM wavenumbers. The harmonic approximation method gives two peak positions at 485.51 cm^{-1} and 548.08 cm^{-1} correspondings to Eu-Ni and Eu-O, respectively. The dopant related vibrational mode due to

Eu-Ni effective mass contribution positioned around 485 cm^{-1} is in between TO and LO mode. Typically, the frequency of the SO phonon modes exhibits dispersion in-between long wavelength LO and TO mode. Interestingly, in the present investigation, the SO mode (445 cm^{-1}) is found to disappear with Eu doping. This disappearance of SO mode with Eu doping can be due to the overlap of SO mode of NiO and LVM due to Eu-Ni effective mass contribution since both of these vibrational modes may appear in between the TO and LO mode [52].

In the present studies, it is interesting that the SO mode of NiO nanostructures found to disappear with Eu-doping, and a remarkable increase in intensity for 1TO and 1LO modes were seen for the $Ni_{0.95}E_{0.5}O$ samples along with 1LO peak broadening. Since the LVM of Eu is around 450 - 550 cm^{-1}, it can influence the SO phonon mode around 445 cm^{-1}. Hence disappearance of SO phonon mode and 1LO peak broadening and enhancement in intensity may be due to the overlapping of SO modes and LVM [52]. The contribution of surface modes in NiO broadens 1LO mode and also the 2LO band [59]. Since the 1LO and 2LO were observed in the Raman spectra, the intensity ratio of 1LO to 2LO (I_{2LO}/I_{1LO}) can be found to estimate the coupling strength [32, 53, 63]. The (I_{2LO}/I_{1LO}) ratio was found to be 0.86 and 0.43 for NiO and $Ni_{0.95}E_{0.5}O$, respectively. The ease off in the coupling strength of $Ni_{0.95}E_{0.5}O$ samples in comparison with pure NiO can be due to the reduction in phonon lifetime that arises due to the defects on the surface [52, 53]. This observation is in accordance with the results obtained from XPS analysis. Besides, with Eu doping, the peak position of the 1M shifts towards lower wavenumber was observed, which may be due to the substitution of larger mass and higher atomic number of Eu compared to the host matrix [57]. This energy shift in the magnon peak can be due to the local symmetry lowering at Ni^{2+} sites resulted from the chemical substitution and vacancies [64]. These outcomes are in good

agreement with the obtained XRD and XPS, which provides the evidence for the chemical substitution of Eu into the NiO lattice.

4. Conclusion

Pure NiO and Eu-doped NiO ($Ni_{0.95}E_{0.5}O$) nanoparticles were synthesized by microwave-assisted hydrothermal method. XRD, Rietveld refinement and EDS analysis confirmed the phase, purity, and the successful substitution of Eu in NiO host material. FE-SEM analysis disclosed porous flake-like morphology in NiO and agglomerated structures in the case of $Ni_{0.95}E_{0.5}O$ samples. XPS investigation revealed the presence of holes and oxygen vacancies in the prepared nanoparticles. Doping with Eu decreases the Ni 3d – O 2p hybridization and increases the concentration of defects in the nanoparticles. Magnetic measurements showed the influence of Eu-doping on the magnetic properties of the nanoparticles. NiO nanoparticles exhibit weak ferromagnetism at low fields due to exchange coupling between uncompensated surface spins and antiferromagnetic core. On doping with Eu, the coercivity and the rate of magnetization were found to increase, which might be due to the change in the number of uncompensated surface spins, reduction in particle size, shape, defects in the prepared nanoparticles, and the effect of spin polarization of the Eu atom. Raman spectroscopy analysis confirmed the presence of defects in the prepared samples. The absence of the 2M band shows antiferromagnetic coupling reduction in the samples. Eu doping produced local vibrations that overlap with the SO mode of NiO and shifting of the 1M band due to its higher mass.

Acknowledgement

Ranjith Kumar P would like to thank the Indo-French Laboratory of Solid-State Chemistry and the CNRS for the financial support. Also, Prof. Bikramjit Basu for his support and A. Hoez, S. Gascoin and F. Veillon are acknowledged for their help during synthesis and

measurements. The authors acknowledge the Micro and Nano Characterization Facility (MNCF), Centre for Nano Science and Engineering (CeNSE), Indian Institute of Science (IISc), Bengaluru, India, for providing the characterization facilities.

References

[1] E. Winkler, R. Zysler, M.V. Mansilla, D. Fiorani, Surface anisotropy effects in NiO nanoparticles, Physical Review B, 72 (2005) 132409.
[2] D. Delgado, B. Solsona, A. Ykrelef, A. Rodríguez-Gómez, A. Caballero, E. Rodríguez-Aguado, E. Rodríguez-Castellón, J. Lopez Nieto, Redox and catalytic properties of promoted NiO catalysts for the oxidative dehydrogenation of ethane, The Journal of Physical Chemistry C, 121 (2017) 25132-25142.
[3] A. Khalil, B.S. Lalia, R. Hashaikeh, Nickel oxide nanocrystals as a lithium-ion battery anode: structure-performance relationship, Journal of Materials Science, 51 (2016) 6624-6638.
[4] H. Duan, X. Zheng, S. Yuan, Y. Li, Z. Tian, Z. Deng, B. Su, Sub-3 nm NiO nanoparticles: Controlled synthesis, and photocatalytic activity, Materials Letters, 81 (2012) 245-247.
[5] P. Liu, V.M.H. Ng, Z. Yao, J. Zhou, Y. Lei, Z. Yang, H. Lv, L.B. Kong, Facile synthesis and hierarchical assembly of flowerlike NiO structures with enhanced dielectric and microwave absorption properties, ACS Applied Materials & Interfaces, 9 (2017) 16404-16416.
[6] R.H. Kodama, S.A. Makhlouf, A.E. Berkowitz, Finite size effects in antiferromagnetic NiO nanoparticles, Physical Review Letters, 79 (1997) 1393.
[7] S.A. Makhlouf, F. Parker, F. Spada, A. Berkowitz, Magnetic anomalies in NiO nanoparticles, Journal of applied physics, 81 (1997) 5561-5563.
[8] A. Emamdoust, S.F. Shayesteh, Surface and electrochemical properties of flower-like Cu-NiO compounds, Journal of Alloys and Compounds, 738 (2018) 432-439.
[9] K.N. Patel, M. Deshpande, K. Chauhan, P. Rajput, V.P. Gujarati, S. Pandya, V. Sathe, S. Chaki, Effect of Mn doping concentration on structural, vibrational and magnetic properties of NiO nanoparticles, Advanced Powder Technology, 29 (2018) 2394-2403.
[10] P. Ponnusamy, S. Agilan, N. Muthukumarasamy, T. Senthil, G. Rajesh, M. Venkatraman, D. Velauthapillai, Structural, optical and magnetic properties of undoped NiO and Fe-doped NiO nanoparticles synthesized by wet-chemical process, Materials Characterization, 114 (2016) 166-171.
[11] J. Al Boukhari, L. Zeidan, A. Khalaf, R. Awad, Synthesis, characterization, optical and magnetic properties of pure and Mn, Fe and Zn doped NiO nanoparticles, Chemical Physics, 516 (2019) 116-124.
[12] V. Biju, M.A. Khadar, Electronic structure of nanostructured nickel oxide using Ni 2p XPS analysis, Journal of Nanoparticle Research, 4 (2002) 247-253.
[13] S. Yousaf, S. Zulfiqar, M.N. Shahi, M.F. Warsi, N.F. Al-Khalli, M.F.A. Aboud, I. Shakir, Tuning the structural, optical and electrical properties of NiO nanoparticles prepared by wet chemical route, Ceramics International, 46 (2020) 3750-3758.
[14] G. George, S. Anandhan, Synthesis and characterisation of nickel oxide nanofibre webs with alcohol sensing characteristics, RSC Advances, 4 (2014) 62009-62020.
[15] J. Li, R. Yan, B. Xiao, D.T. Liang, D.H. Lee, Preparation of nano-NiO particles and evaluation of their catalytic activity in pyrolyzing biomass components, Energy & Fuels, 22 (2007) 16-23.

[16] S.K. Meher, P. Justin, G. Ranga Rao, Microwave-mediated synthesis for improved morphology and pseudocapacitance performance of nickel oxide, ACS Applied Materials & Interfaces, 3 (2011) 2063-2073.
[17] S. Vijayakumar, S. Nagamuthu, G. Muralidharan, Supercapacitor studies on NiO nanoflakes synthesized through a microwave route, ACS applied materials & interfaces, 5 (2013) 2188-2196.
[18] J. Zhang, D. Zeng, Q. Zhu, J. Wu, Q. Huang, C. Xie, Effect of nickel vacancies on the room-temperature NO2 sensing properties of mesoporous NiO nanosheets, The Journal of Physical Chemistry C, 120 (2016) 3936-3945.
[19] J.-C.G. Bünzli, S. Comby, A.-S. Chauvin, C.D. Vandevyver, New opportunities for lanthanide luminescence, Journal of rare earths, 25 (2007) 257-274.
[20] J. Chauhan, U. Chaubey, Synthesis and Characterization of Neodymium Doped Nickel Oxide Nanoparticles, Synthesis, 8 (2018).
[21] J. Al Boukhari, A. Khalaf, R. Sayed Hassan, R. Awad, Structural, optical and magnetic properties of pure and rare earth-doped NiO nanoparticles, Applied Physics A, 126 (2020) 1-13.
[22] J. Al Boukhari, A. Khalaf, R. Awad, Structural and electrical investigations of pure and rare earth (Er and Pr)-doped NiO nanoparticles, Applied Physics A, 126 (2020) 74.
[23] J. Al Boukhari, A. Khalaf, R. Awad, Structural analysis and dielectric investigations of pure and rare earth elements (Y and Gd) doped NiO nanoparticles, Journal of Alloys and Compounds, 820 (2020) 153381.
[24] J. Al Boukhari, R.S. Hassan, R. Awad, Improving the dielectric behavior of NiO nanoparticles by Samarium doping for electromagnetic applications, Materials Research Express, 6 (2019) 115094.
[25] M.N. Siddique, A. Ahmed, S. Riyajuddin, M. Faizan, K. Ghosh, P. Tripathi, Exploring the Ce3+ ions doping effect on optical and magnetic properties of NiO nanostructures, Journal of Magnetism and Magnetic Materials, 500 (2020) 166323.
[26] W. Dai, Mechanism of the reduction and energy transfer between Eu 2+ and Eu 3+ in Eu-doped CaAl 2 Si 2 O 8 materials prepared in air, Journal of Materials Chemistry C, 2 (2014) 3951-3959.
[27] S. Goumri-Said, W. Khan, K. Boubaker, G. Turgut, E. Sönmez, J. Minar, M. Bououdina, M.B. Kanoun, Europium incorporation dynamics within NiO films deposited by sol-gel spin coating: experimental and theoretical studies, Materials Research Bulletin, (2019) 110525.
[28] S. Komarneni, R. Roy, Q. Li, Microwave-hydrothermal synthesis of ceramic powders, Materials Research Bulletin, 27 (1992) 1393-1405.
[29] M. Farbod, M.Z. Shoushtari, Size dependence of optical and magnetic properties of nickel oxide nanoparticles fabricated by electric arc discharge method, Ceramics International, 43 (2017) 13670-13676.
[30] L. Lutterotti, Total pattern fitting for the combined size–strain–stress–texture determination in thin film diffraction, Nuclear Instruments and Methods in Physics Research Section B: Beam Interactions with Materials and Atoms, 268 (2010) 334-340.
[31] V. Mote, Y. Purushotham, B. Dole, Williamson-Hall analysis in estimation of lattice strain in nanometer-sized ZnO particles, Journal of Theoretical and Applied Physics, 6 (2012) 6.
[32] W. Duan, S. Lu, Z. Wu, Y. Wang, Size effects on properties of NiO nanoparticles grown in alkalisalts, The Journal of Physical Chemistry C, 116 (2012) 26043-26051.
[33] N. Rinaldi-Montes, P. Gorria, D. Martínez-Blanco, A.B. Fuertes, I. Puente-Orench, L. Olivi, J.A. Blanco, Size effects on the Néel temperature of antiferromagnetic NiO nanoparticles, AIP advances, 6 (2016) 056104.

[34] S. Popkov, A. Krasikov, A. Dubrovskiy, M. Volochaev, V. Kirillov, O. Martyanov, D. Balaev, Size effects in the formation of an uncompensated ferromagnetic moment in NiO nanoparticles, Journal of Applied Physics, 126 (2019) 103904.
[35] C.A. Schneider, W.S. Rasband, K.W. Eliceiri, NIH Image to ImageJ: 25 years of image analysis, Nature methods, 9 (2012) 671.
[36] A. Manikandan, J.J. Vijaya, L.J. Kennedy, Comparative investigation of NiO nano-and microstructures for structural, optical and magnetic properties, Physica E: Low-Dimensional Systems and Nanostructures, 49 (2013) 117-123.
[37] K. Maniammal, G. Madhu, V. Biju, X-ray diffraction line profile analysis of nanostructured nickel oxide: Shape factor and convolution of crystallite size and microstrain contributions, Physica E: Low-dimensional Systems and Nanostructures, 85 (2017) 214-222.
[38] M.C. Biesinger, B.P. Payne, A.P. Grosvenor, L.W. Lau, A.R. Gerson, R.S.C. Smart, Resolving surface chemical states in XPS analysis of first row transition metals, oxides and hydroxides: Cr, Mn, Fe, Co and Ni, Applied Surface Science, 257 (2011) 2717-2730.
[39] E. Khawaja, M. Salim, M. Khan, F. Al-Adel, G. Khattak, Z. Hussain, XPS, auger, electrical and optical studies of vanadium phosphate glasses doped with nickel oxide, Journal of non-crystalline solids, 110 (1989) 33-43.
[40] B. Zou, L. Wang, J. Lin, The electronic structures of NiO nanoparticles coated with stearates, Solid state communications, 94 (1995) 847-850.
[41] G. Allen, S. Harris, J. Jutson, J. Dyke, A study of a number of mixed transition metal oxide spinels using X-ray photoelectron spectroscopy, Applied Surface Science, 37 (1989) 111-134.
[42] B. Payne, M. Biesinger, N. McIntyre, Use of oxygen/nickel ratios in the XPS characterisation of oxide phases on nickel metal and nickel alloy surfaces, Journal of Electron Spectroscopy and Related Phenomena, 185 (2012) 159-166.
[43] F. Mercier, C. Alliot, L. Bion, N. Thromat, P. Toulhoat, XPS study of Eu (III) coordination compounds: Core levels binding energies in solid mixed-oxo-compounds EumXxOy, Journal of electron spectroscopy and related phenomena, 150 (2006) 21-26.
[44] S. Kumar, R. Prakash, R. Choudhary, D. Phase, Structural, XPS and magnetic studies of pulsed laser deposited Fe doped Eu2O3 thin film, Materials Research Bulletin, 70 (2015) 392-396.
[45] P. Zhang, Y. Zhao, T. Zhai, X. Lu, Z. Liu, F. Xiao, P. Liu, Y. Tong, Preparation and magnetic properties of polycrystalline Eu2O3 microwires, Journal of the Electrochemical Society, 159 (2012) D204-D207.
[46] A. Berkowitz, R. Kodama, S.A. Makhlouf, F. Parker, F. Spada, E. McNiff Jr, S. Foner, Anomalous properties of magnetic nanoparticles, Journal of magnetism and magnetic materials, 196 (1999) 591-594.
[47] K. Moura, R. Lima, A. Coelho, E. Souza-Junior, J. Duque, C. Meneses, Tuning the surface anisotropy in Fe-doped NiO nanoparticles, Nanoscale, 6 (2014) 352-357.
[48] N. Prasad, B. Karthikeyan, Phase-dependent structural, optical, phonon and UV sensing properties of ZnS nanoparticles, Nanotechnology, 30 (2019) 485702.
[49] N. Prasad, B. Karthikeyan, A Raman spectral probe on polar w-ZnS nanostructures and surface optical phonon modes in nanowires, Nanoscale, 11 (2019) 4948-4958.
[50] B.J. Rani, B. Saravanakumar, G. Ravi, V. Ganesh, A. Sakunthala, R. Yuvakkumar, Structural, optical and magnetic properties of NiO nanopowders, Journal of nanoscience and nanotechnology, 18 (2018) 4658-4666.
[51] E. Aytan, B. Debnath, F. Kargar, Y. Barlas, M. Lacerda, J. Li, R. Lake, J. Shi, A. Balandin, Spin-phonon coupling in antiferromagnetic nickel oxide, Applied Physics Letters, 111 (2017) 252402.

[52] N. Prasad, K. Balasubramanian, Raman spectral probe on increased local vibrational modes and phonon lifetimes in Ho3+-doped Bi2O3 micro-rods, Journal of Raman Spectroscopy, 47 (2016) 1266-1270.
[53] J. Sarkar, S.G. Menon, N. Prasad, B. Karthikeyan, N. Kamaraju, Ultrafast Carrier Dynamics of Undoped and Ho3+-Doped α-Bismuth Oxide Microrods, The Journal of Physical Chemistry C, 123 (2019) 10007-10012.
[54] P. Ravikumar, B. Kisan, A. Perumal, Enhanced room temperature ferromagnetism in antiferromagnetic NiO nanoparticles, Aip Advances, 5 (2015) 087116.
[55] B. Zhao, J. Song, P. Liu, W. Xu, T. Fang, Z. Jiao, H. Zhang, Y. Jiang, Monolayer graphene/NiO nanosheets with two-dimension structure for supercapacitors, Journal of Materials Chemistry, 21 (2011) 18792-18798.
[56] W. Wang, Y. Liu, C. Xu, C. Zheng, G. Wang, Synthesis of NiO nanorods by a novel simple precursor thermal decomposition approach, Chemical Physics Letters, 362 (2002) 119-122.
[57] A.C. Gandhi, H.-Y. Cheng, Y.-M. Chang, J.G. Lin, Size confined magnetic phase in NiO nanoparticles, Materials Research Express, 3 (2016) 035017.
[58] G.A. Babu, G. Ravi, M. Navaneethan, M. Arivanandhan, Y. Hayakawa, An investigation of flower shaped NiO nanostructures by microwave and hydrothermal route, Journal of Materials Science: Materials in Electronics, 25 (2014) 5231-5240.
[59] N. Mironova-Ulmane, A. Kuzmin, I. Sildos, L. Puust, J. Grabis, Magnon and Phonon Excitations in Nanosized NiO, Latvian Journal of Physics and Technical Sciences, 56 (2019) 61-72.
[60] N. Mironova-Ulmane, A. Kuzmin, I. Sildos, M. Pärs, Polarisation dependent Raman study of single-crystal nickel oxide, Central European Journal of Physics, 9 (2011) 1096-1099.
[61] M. McCluskey, Local vibrational modes of impurities in semiconductors, Journal of Applied Physics, 87 (2000) 3593-3617.
[62] A. Sunny, K. Balasubramanian, Raman Spectral Probe on Size Dependent Surface Optical Phonon Modes and Mangnon Properties of NiO Nanoparticle, The Journal of Physical Chemistry C, (2020).
[63] F. Ascencio, A. Bobadilla, R. Escudero, Study of NiO nanoparticles, structural and magnetic characteristics, Applied Physics A, 125 (2019) 279.
[64] I. Kolesnikov, A. Povolotskiy, D. Mamonova, E. Lähderanta, A. Manshina, M. Mikhailov, Photoluminescence properties of Eu 3+ ions in yttrium oxide nanoparticles: defect vs. normal sites, RSC Advances, 6 (2016) 76533-76541.
[65] R. Udayabhaskar, B. Karthikeyan, Role of micro-strain and defects on band-gap, fluorescence in near white light emitting Sr doped ZnO nanorods, Journal of Applied Physics, 116 (2014) 094310.

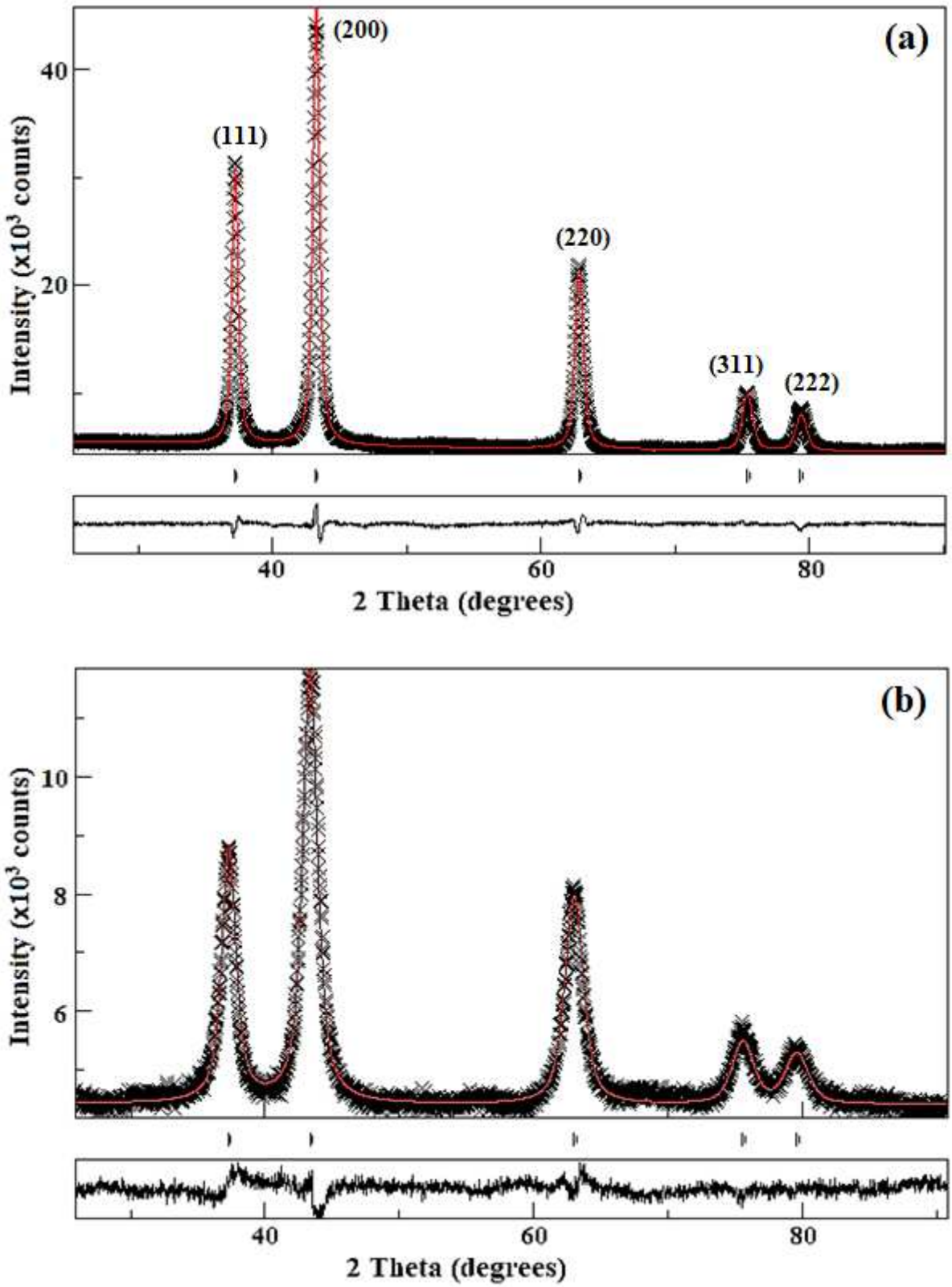

Figure 1. Refined x-ray diffraction pattern of (a) pure NiO and (b) Eu-doped NiO nanoparticles.

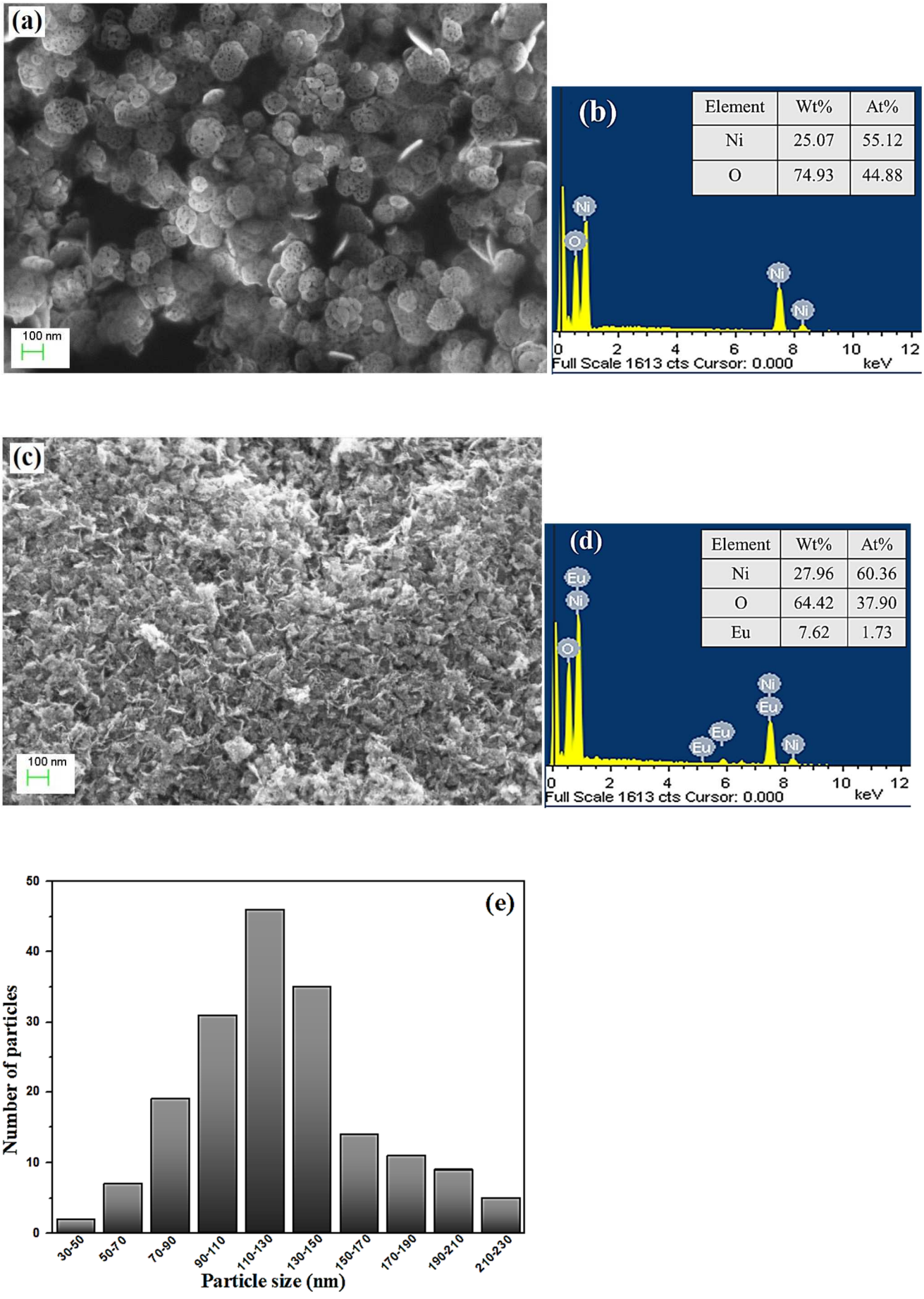

Figure 2. SEM image and the corresponding EDS of (a) undoped and (b) doped NiO nanoparticles (c) and (d). Particle size distribution of undoped NiO nanoparticles.

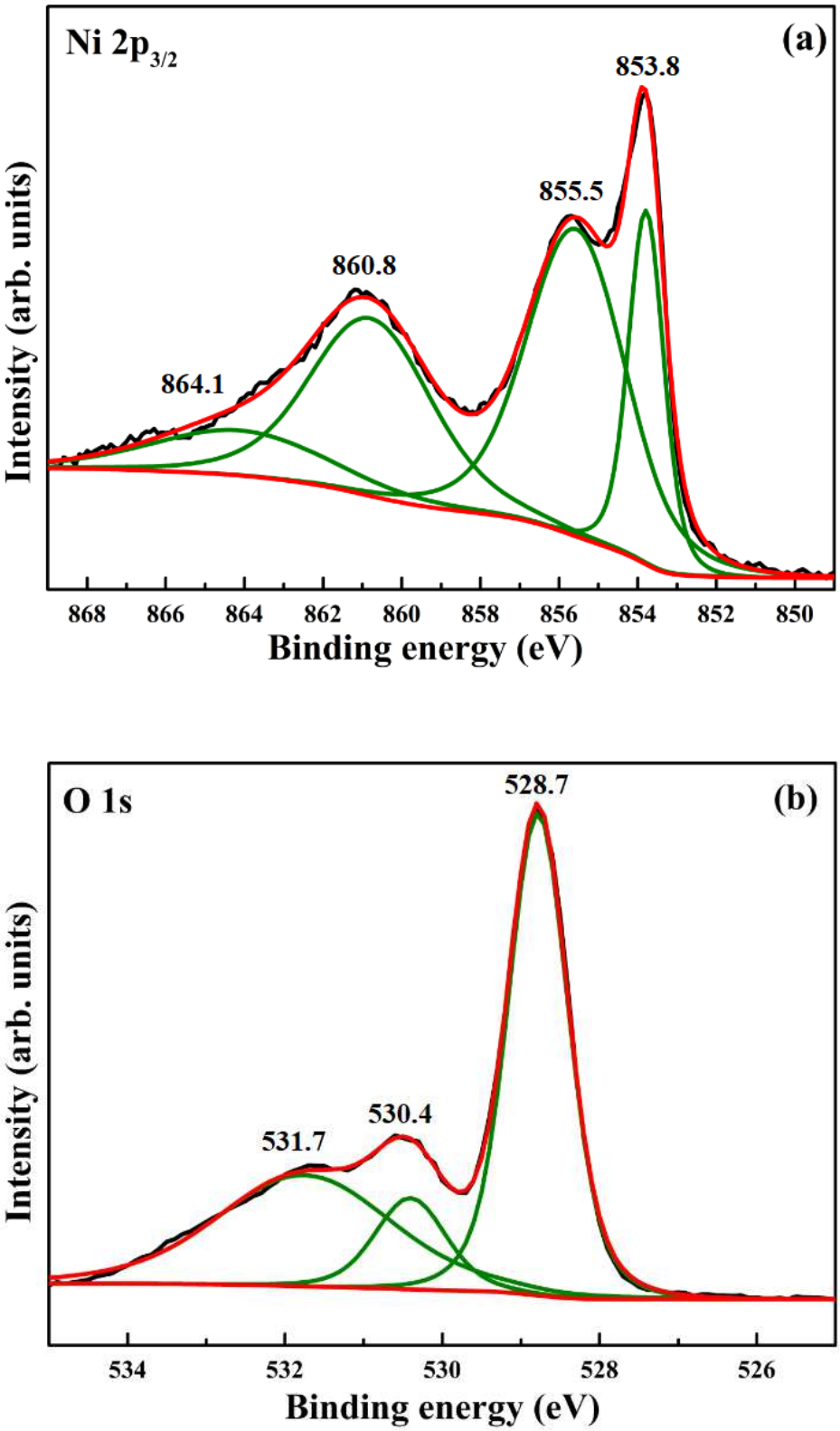

Figure 3. Core level XPS spectra of (a) Ni $2p_{3/2}$ and (b) O 1s of undoped NiO nanoparticles.

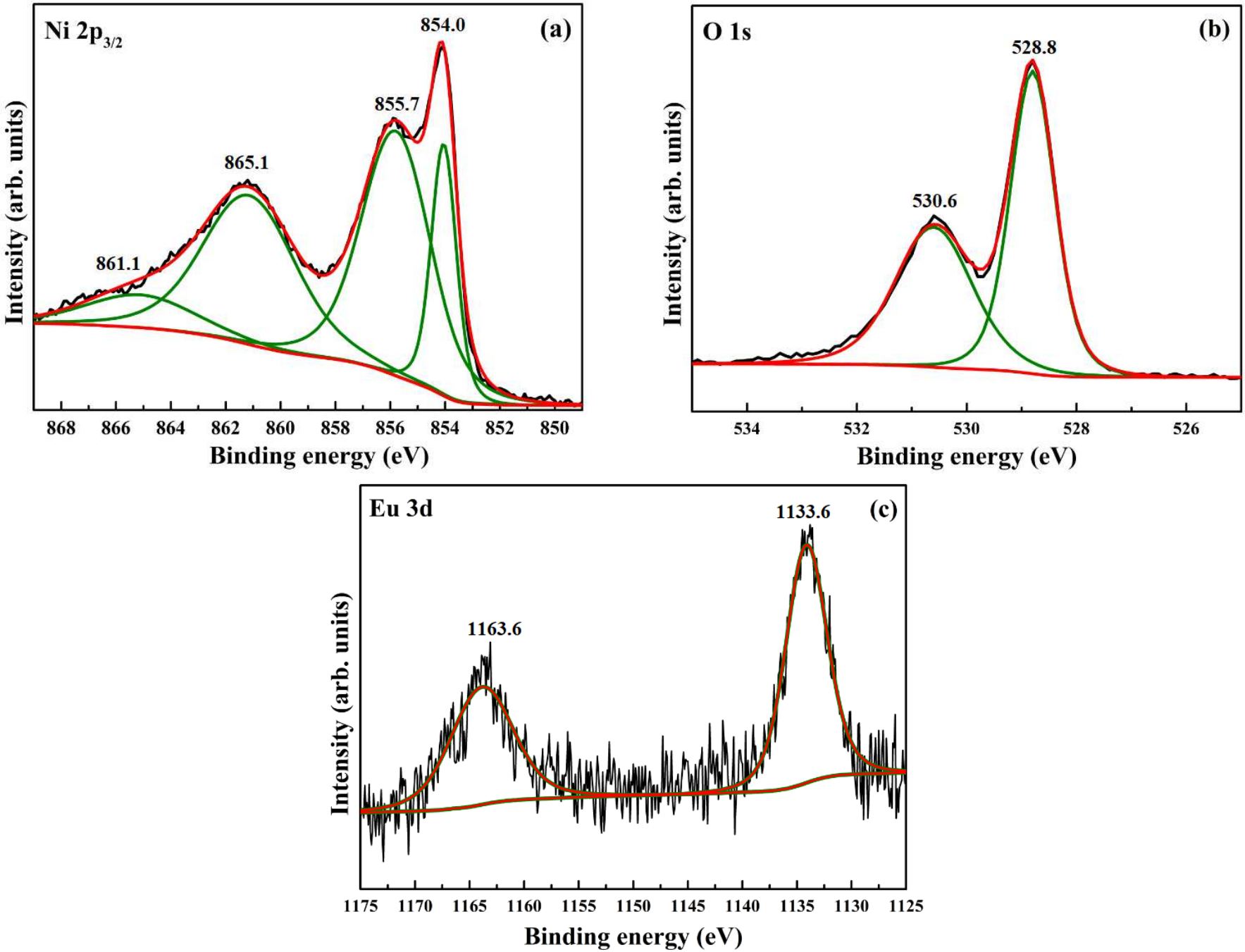

Figure 4. Core level XPS spectra of (a) Ni $2p_{3/2}$, (b) O 1s and (c) Eu 3d of doped NiO nanoparticles.

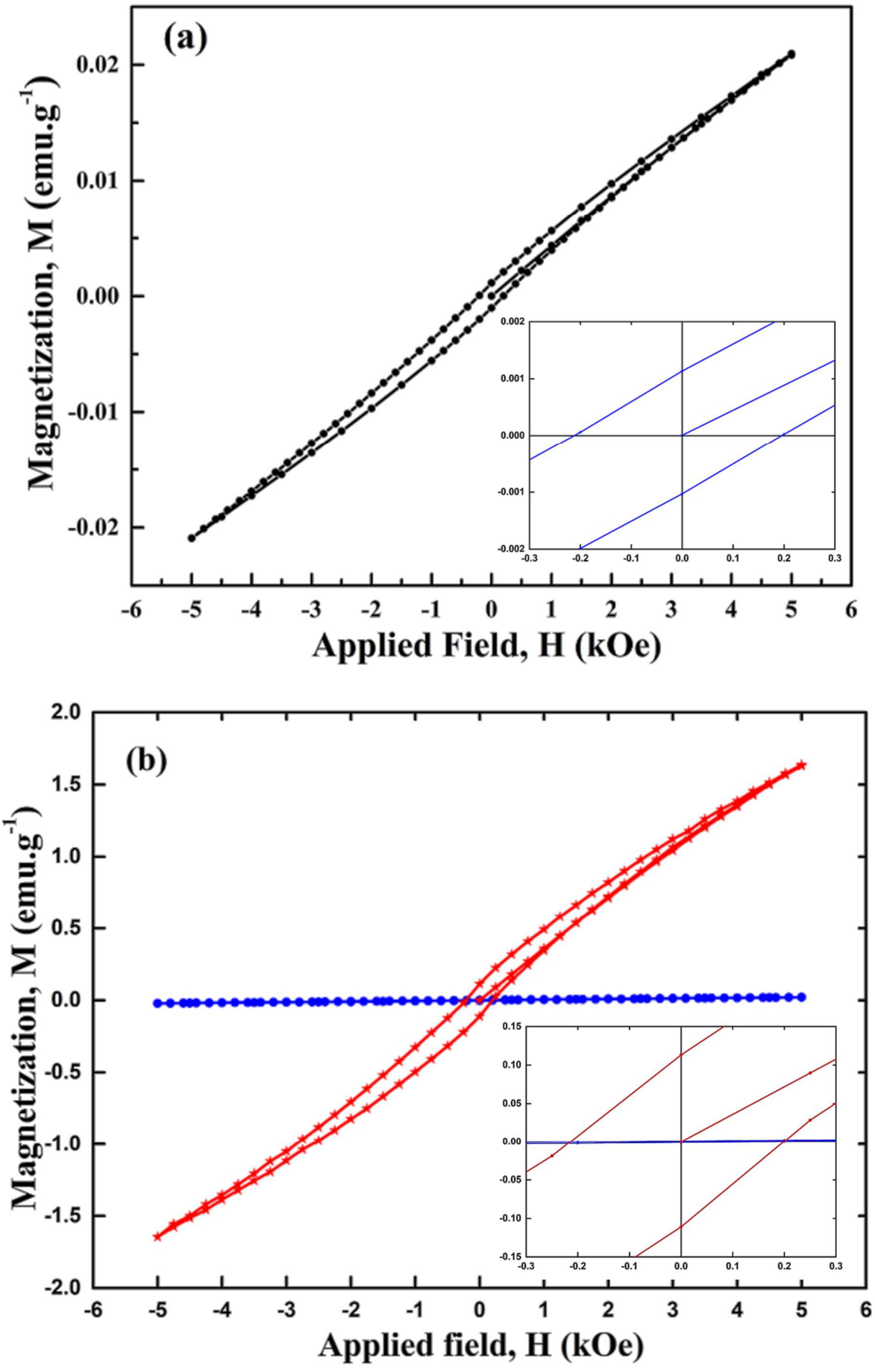

Figure 5. Hysteresis loops of (a) undoped, and (b) Eu doped NiO nanoparticles at room temperature.

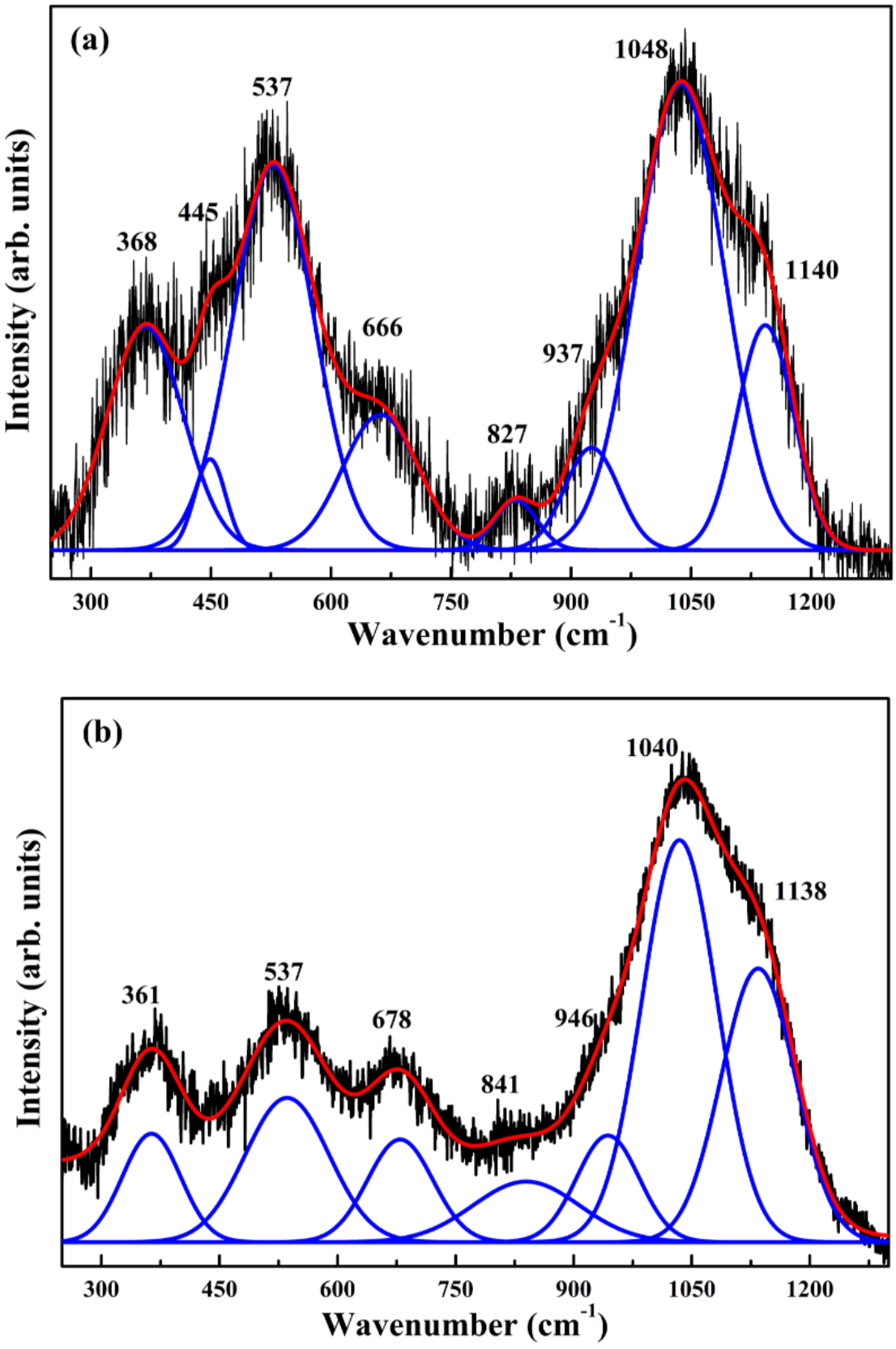

Figure 6. Room temperature Raman spectra of (a) undoped and (b) doped NiO nanoparticles.

Table 1. Rietveld refined parameters of the prepared nanoparticles

Sample	**R_{wp} (%)**	**R_{exp} (%)**	**Lattice parameter (Å)**		**Crystallite size (nm)**
			Calculated	**Refined**	
NiO	2.34	1.27	4.17	4.17	13.45
$Ni_{0.95}E_{0.5}O$	2.19	1.42	4.18	4.18	6.51

Table 2. Summary of XPS results of the prepared nanoparticles

Sample	**Element**	**Peak energy (eV)**	**Peak width FWHM (eV)**	**Peak Area (eV×cps)**
NiO	Ni $2p_{3/2}$	853.8	1.1	4613.7
		855.5	2.9	10159.4
		860.8	3.8	8006.0
		864.1	5.1	2366.2
	O 1s	528.7	0.9	4277.7
		530.4	1.1	947.5
		531.7	2.6	2856.3
$Ni_{0.95}E_{0.5}O$	Ni $2p_{3/2}$	854.0	1.1	2245.0
		855.7	2.9	5769.6
		861.1	3.9	4394.3
		865.1	5.4	1419.7
	O 1s	528.8	0.9	2438.5
		530.6	1.7	1958.6
	Eu 3d	1133.6	4.5	1233.8
		1163.6	6.7	825.3